Journal of Structural Geology, Vol. 3, No. 4, pp. 421 to 436, 1981.
Printed in Great Britain

0191-8141/81/040421-16 $02.00/0

Strain analysis of a Northern Apennine shear zone using deformed marble breccias

ROY KLIGFIELD

Geologisches Institut, ETH-Zentrum, CH-8092 Zürich, Switzerland

L. CARMIGNANI

Istituto di Geologia, Via S. Maria 53, Pisa, Italia

and

W. H. OWENS

Department of Geological Sciences, University of Birmingham, England

(*Received* 19 *January* 1981; *accepted in revised form* 5 *June* 1981)

Abstract—The Alpi Apuane region of the Northern Apennines appears to have been deformed within a large-scale, low-angle shear zone with an overthrust sense of movement. The presence of mineral stretching lineations, folds progressively rotated into the X strain direction, and schistosities which intersect the nappe boundaries at small angles suggest that a component of shear strain occurred during the deformation. The strain ratios and orientations on two-dimensional sections have been determined from deformed marble breccias, reduction spots, and oncalites. Data from three or more non-perpendicular, non-principal sections have been combined to determine the finite strain ellipsoids at 33 sites within the shear zone.

The finite strains have been separated into components of simple shear (γ), longitudinal strain (λ), and volume change (Δ). Algebraic expressions have been derived and graphs constructed which enable components of γ, γ and Δ, and γ and λ to be determined directly from a knowledge of strain ratio (R) within the shear zone and the angle (θ) between the principal strain direction and the shear zone boundary. The Alpi Apuane data indicate that neither simple shear alone, nor simple shear with volume change can satisfactorily explain the observed strains. Consideration of simple shear plus longitudinal strain leads to a general relationship in which the value of shear increases, and the values of longitudinal strain change along a SW–NE profile across the zone. Integration of the resulting shear strain–distance curves gives a minimum displacement of 4 km within the shear zone. Combination of the finite strains with the total time of deformation known from K/Ar studies leads to average strain rates from 1.4 to 9.6 $\times$ 10^{-15} sec^{-1}.

A characteristic flat–ramp–flat geometry initially formed the boundaries of what was later to develop into the overthrust shear zone, and deformation of the underlying crystalline basement is believed to have occurred by ductile shearing. Estimates of 21% crustal shortening for the region suggest that the crustal thickness prior to deformation was approximately 20 km in this part of the Northern Apennines.

Riassunto—Le Alpi Apuane sono una regione deformata in una zona di taglio alla base delle falde alloctone dell'Appennino settentrionale. Marcate lineazioni di estensione, pieghe progressivamente ruotate nella direzione di massima estensione e scistosita che interseca con basso angolo la base dell'unità alloctona sovrastante, suggeriscono una componente di taglio semplice nella deformazione. Su sezioni bidimenzionali sono stati determinati i rapporti e l'orientazione degli strains principali dell'ellisse dello strain in brecce di marmo deformate, reduction spots e oncoliti. I risultati ottenuti per tre o più sezioni non perpendicolari e non principali sono stati combinati per determinare l'ellissoide dello strain finito in 33 località.

Gli strains finiti sono stati divisi in componenti di strain di taglio (γ), strain longitudinale (λ), e variazione di volume (Δ). Attraverso espressioni algebriche e diagrammi sono state determinate le componenti di γ, di γ e Δ, e di γ e λ, conoscendo i rapporti degli strains principali (R) nella zona di taglio e l'angolo (θ) tra la direzione dello strain principale massimo e il limite della zona di taglio. I dati delle Alpi Apuane indicano che ne il taglio semplice da solo, ne il taglio semplice accompagnato da variazioni di volume può spiegare completamente i valori di strain finito misurati. Considerando taglio semplice più strain longitudinale si arriva a une distribuzione delle componenti dello strain, lungo un profilo SW–NE attraverso la zona di taglio, in cui il valore dello strain di taglio aumenta, e il tipo dello strain longitudinale passa dall'appiattimento alla costrizione. L'integrale della curva strain di taglio–distanza mostra uno spostamento minimo di circa 4 km per deformazione continua dentro la zona di taglio. I valori di strain finito e la durata complessiva della deformazione stimata attraverso determinazioni K/Ar suggeriscono tassi medi di strain da 1,4 a 9,6 $\times$ 10^{-15} sec^{-1}.

I valori di strain finito e la distribuzione degli affioramenti nelle Apuane metamorfiche suggeriscono che la geometria iniziale del contatto tettonico, da cui si é successivamente sviluppato l'accavallamento e la zona di taglio, avesse brusche variazioni di inclinazione passando dalle formazioni più competenti alle meno competenti della copertura (flat–ramp–flat geometry) mentre la deformazione nel basamento cristallino é probabile procedesse per taglio duttile. La stima del raccorciamento crustale attorno al 21% suggerisce che lo spessore della crosta in questa segmento dell'Appennino fosse di circa 20 km prima della deformazione.

INTRODUCTION

LARGE portions of the Alps, Apennines and Himalayas have undergone considerable crustal shortening during the collisional deformation of continental margins following ophiolite subduction and suturing. Common to these regions is the presence of numerous sedimentary sequences of both oceanic and continental margin facies now found stacked as allochthonous sheets above the adjacent continental margin.

In order to investigate the mechanisms responsible for this crustal shortening, it is necessary to acquire quantitative data on the internal changes in shape that these sheets have undergone. Limestone breccias which originally formed as syn-sedimentary fault scarp deposits occur in the Northern Apennines. These breccias were deformed and metamorphosed within the limits of a large-scale, low-angle, overthrust-sense shear zone during the Tertiary collisional deformation of the Northern Apennines. This work: (1) investigates the use of these marble breccias as strain markers; (2) discusses the relationships of the finite strain results to the shear zone geometry; (3) provides quantitative estimates for the amounts of displacement, crustal shortening, and strain rates in this part of the Northern Apennines and (4) discusses a deformation model in which Northern Apennine crustal shortening is accommodated largely by the formation of shear zones in basement and cover.

GEOLOGIC SETTING

In the Northern Apennines, ophiolite sequences and their sedimentary cover are found in allochthonous positions above rocks of continental margin and platform carbonate facies. In regions such as Punta Bianca, Alpi Apuane, and Mt. Pisani (Fig. 1) the basement is exposed in a series of tectonostratigraphic sequences, which are, in ascending structural order: (1) the Tuscan metamorphic sequences; (2) the Tuscan nappe and (3) the overlying Liguride units (Gianinni & Lazzarotto 1975, Carmignani *et al.* 1978).

The Tuscan metamorphic sequences consist of Upper Carboniferous (Rau & Tongiorgi 1974) to Oligocene metasediments resting unconformably on a Palaeozoic basement which has been affected by Hercynian deformation. In the Mesozoic portion of this sequence, marble breccias are found in different stratigraphic positions (Fig. 2): (a) as polygenetic breccias between the Upper Triassic dolomite and Lower Liassic marble (marble and dolomite clasts in a carbonate/pelagic matrix) (Giglia & Trevisan 1966); (b) as monogenetic breccias found within Lower Liassic marbles (marble clasts in a carbonate matrix); and (c) as monogenetic and polygenetic breccias between the Lower Liassic marbles and Middle–Upper Liassic cherty limestones (marble clasts in a carbonate matrix). The rocks at Punta Bianca and in the westernmost part of the Alpi Apuane region (known as the Massa unit) have a different sedimentation history. Here, monogenetic breccias (marble clasts in a pelitic/carbonate matrix) are found in the Middle Triassic.

We interpret these breccias to be the products of activity along syn-sedimentary block faults during the Mesozoic evolution of this part of the Apennine continental margin (Bernoulli *et al.* 1979). Very similar megabreccias are known from the Central Apennines where the general absence of metamorphism and deformation provides the possibility of observing their predeformation geometries (Colacicchi *et al.* 1975). According to these authors, tectonic activity on steep faults produced the megabreccia accumulations. The general fabric is chaotic and no primary sedimentary structure is recognizable. The apparent lack of initial fabric and absence of significant competence differences between clasts and matrix provide an outstanding opportunity to use these breccias as strain markers.

BRECCIA DEFORMATION

Deformation of both Palaeozoic basement and the Upper Carboniferous to Oligocene cover in the metamorphic sequences is intense, penetrative and polyphase. In

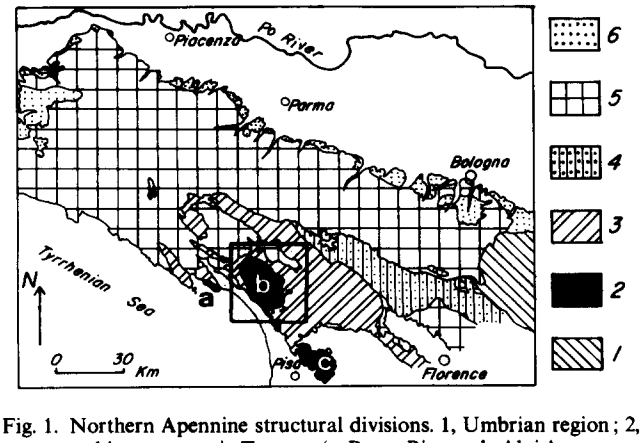

Fig. 1. Northern Apennine structural divisions. 1, Umbrian region; 2, metamorphic sequences in Tuscany (a, Punta Bianca; b, Alpi Apuane; c, Mt. Pisano); 3, Tuscan nappe; 4, Cervarola flysch; 5, Liguride sequences; 6, Miocene–Pliocene sediments. Location of Fig. 4 indicated by the rectangle.

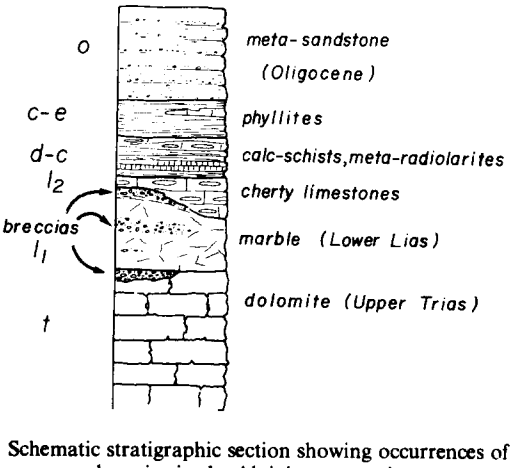

Fig. 2. Schematic stratigraphic section showing occurrences of marble breccias in the Alpi Apuane region.

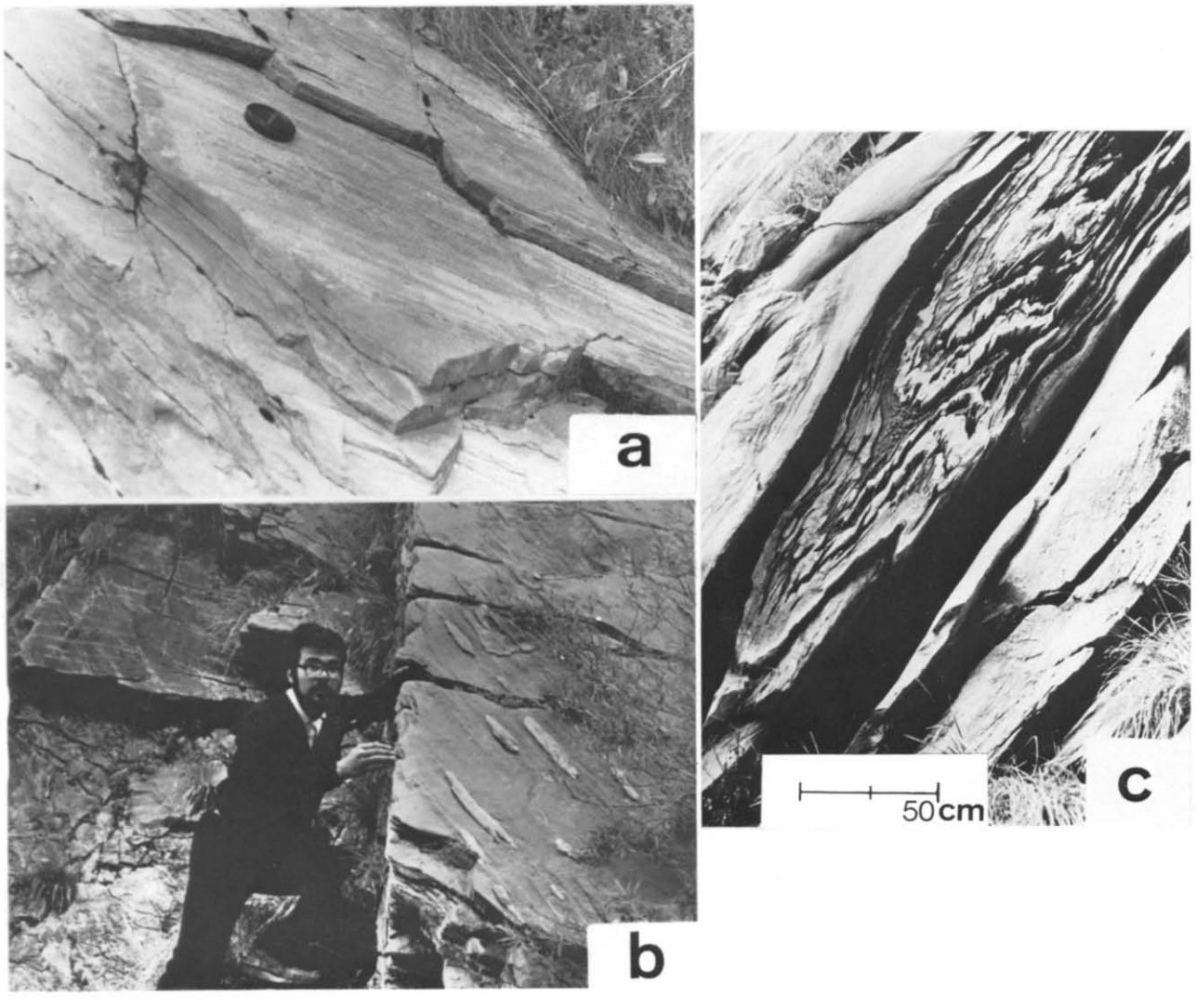

Fig. 3. Progressive changes in D_1-phase fold geometry in the SW to NE cross sections of Fig. 8. (a) Mineral extension lineation (L_1) in marble, trends WSW to ENE within the S_1 schistosity. Diameter of lens-cap is 5 cm. (b) Rotated folds in cherty limestone from the eastern part of cross section (locality 5 of Figs. 4 and 8). D_1 fold hinge lines are parallel to the down-dip L_1 lineation. The bedding is completely transposed into schistosity and the folds in chert layers have the characteristic appearance of sheath folds. (c) Non-rotated folds in cherty limestone from the western part of cross sections (locality 8 of Figs. 4 and 8). D_1-phase fold hinge lines lie sub-horizontal within S_1, but are perpendicular to the down-dip L_1 lineation.

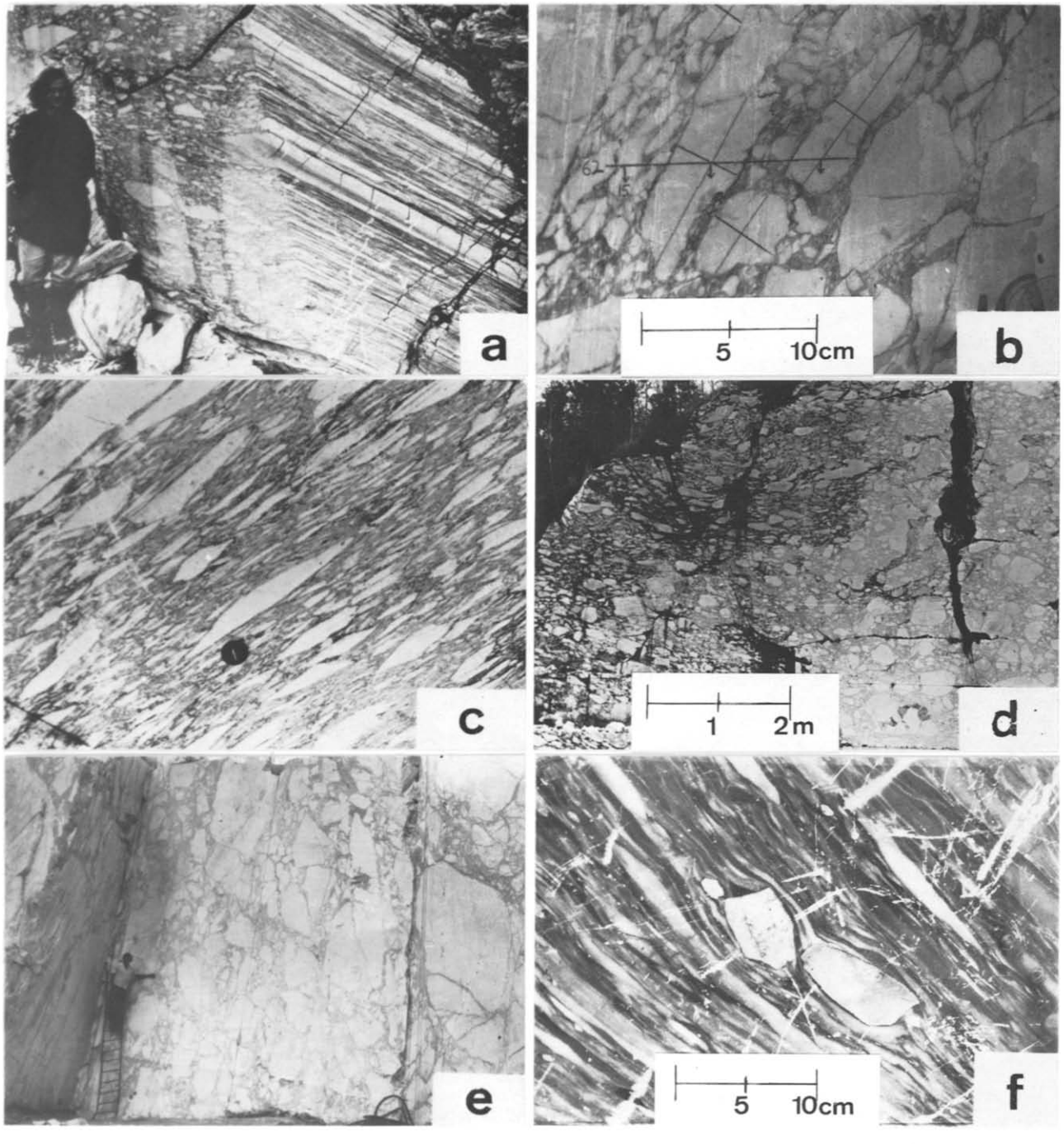

Fig. 5. Northern Apennine marble breccias. (a) Marble breccia block showing change in appearance of three-dimensional geometry on planar sections oriented at right angles to each other. (b) Planar section showing R_f/ϕ method of measurement. Note pressure solution effects on marble clast boundaries. (c) XZ section (lens-cap is 5 cm diameter). (d) YZ section showing elongation in X direction (horizontal, into face). (e) Quarry section which is nearly a circular section of the finite strain ellipsoid, showing the original pre-deformation shapes of the breccias. (f) Breccia between Triassic dolomite and lower Liassic marble. Dolomite clasts (centre) show large competence difference with matrix, while marble clasts show no evidence of competence difference.

the main deformation phase (D_1), the metamorphic sequences were deformed into tight, recumbent folds with gently dipping axial surfaces. An axial planar schistosity (S_1) developed, containing a WSW–ENE trending mineral extension lineation (L_1) (Fig. 3a). Subsequent phases (post nappe-emplacement) refolded all tectonic contacts and produced open, asymmetric folds. The geometries of the different deformation phases have been described in detail by Carmignani *et al.* (1978) and Carmignani & Giglia (1977, 1979a, 1979b).

A progressive 90° change in the orientation of first phase fold axes (A_1) is seen from WSW to ENE across the region (Figs. 3 and 4). The A_1 fold axes in the western region trend NW–SE and are subhorizontal (Fig. 3c) while the L_1 lineation plunges down-dip within the S_1 schistosity at 90° to fold axes. In the eastern region, A_1 fold axes are parallel to the down-dip mineral extension lineation (Fig. 3b) and the strongly appressed folds resemble sheath folds (Cobbhold & Quinquis 1980). This relationship has been proposed (Carmignani *et al.* 1978) as an example of passive rotation of early-formed folds into the extension direction during progressive simple shear (Sanderson 1973, Escher & Watterson 1974, Rhodes & Gayer 1977, Williams 1978). In such a model, the schistosities orientated at a small angle to the overlying nappe boundaries, the progressive rotation of folds into the extension direction, and the strongly-developed mineral extension lineations were developed within the confines of a large scale, low-angle shear zone with an overthrust sense of motion (Kligfield 1979).

The breccia shapes (axes $X > Y > Z$) reflect the geometry of the D_1 deformation phase (Fig. 5). The breccias are flattened within the S_1 schistosity and are elongated parallel to the L_1 mineral extension lineation as measured in the surrounding matrix material. Little or no competence difference is apparent between marble clasts and matrix (Fig. 5f). Some marble clasts are found immersed in a cleaved, formerly muddy matrix. In these cases the S_1 schistosity in the matrix material passes without deviation into the XY plane of the breccias.

The original breccia fabric has been folded during a late (D_3) deformation phase (Carmignani *et al.* 1978). The relative development of this phase, which is not penetratively developed throughout the region, varies from

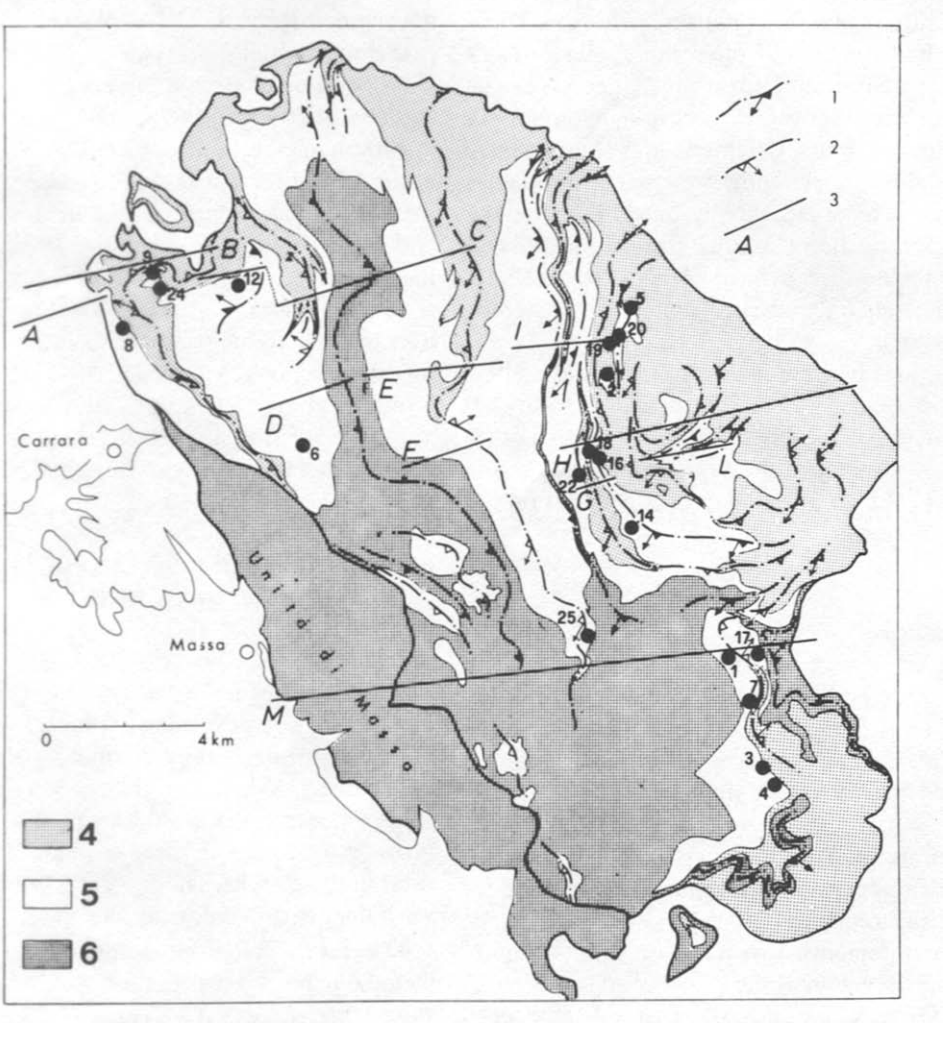

Fig. 4. Structural sketch map of Alpi Apuane metamorphic sequences. Localities of sites where strain values were determined are indicated by numbered dots. Key to legend: 1, axial plane traces of D_1-phase anticlines with plunge of fold axes; 2, axial plane trace of D_1 synclines with plunge of fold axes; 3, traces of cross sections of Fig. 8; 4, Dogger to Oligocene strata; 5, outcrops of Liassic marbles; 6, Palaeozoic to Triassic strata.

place to place. Its overall effect is to reorient the S_1 schistosity and breccia fabric; even in areas of strong refolding the breccias do not appear to have taken on much incremental strain related to the D_3 phase. In extreme cases, the D_3 deformation has completely modified the breccia shapes. The effects of this phase on the strain analysis is discussed later.

Pressure solution effects are also evident on the boundaries of some clasts. However due to the greenschist facies metamorphism, some stylolites and insoluble residue seams appear to have been refolded in a ductile manner. No attempt has been made in this analysis to measure separately the shape change due to pressure solution. The strain measurements therefore represent the total distortions due to both plastic deformation and pressure solution.

STRAIN ANALYSIS

It has been possible to measure the state of strain using different strain markers from the same region. Marble breccia quarries are present throughout the region and provide exceptionally good exposures. The marble breccia is cut *in situ* into planar sections using wire saws. There are usually at least three, and often more, quarry faces having different orientations and on which breccias can be measured. Reduction spots are occasionally found in Eocene varicoloured shales. Oriented block samples have been cut in the laboratory along principal strain planes and the spot shapes recorded. Finally, oncalites within the Liassic marbles have been used as strain indicators at locality 12. Oncalites are a form of algal stromatolite whose original geometry consists of concentric spheroids (Logan *et al.* 1964).

Strain measurements were made at only 1 site each in the Punta Bianca (locality 15) and Mt. Pisani (locality 13) areas (Fig. 1), mainly for comparison purposes. All other measurements were made in the Alpi Apuane region; the site localities are shown in the map of Fig. 4 and on the cross sections of Fig. 8.

Two-dimensional strain analyses

All measurements were made directly in the field on the marble quarry faces. For a selected number of sites, the ratio of breccia long and short axis lengths (R_f) and the angle (ϕ) which the long axis makes with a reference direction in the section plane were measured (Fig. 5b). At the beginning of the study as many as 200 measurements per section were made; later this number was reduced to about 30–50 measurements (Table 1).

The R_f/ϕ measurements were made on three or more sections in order to examine the range of initial breccia ratios (R_i), to check for the presence of any pre-deformation preferred orientation of the breccia long axes (θ), and to determine the finite strain ratios (R_s) on each section. The data were analysed at first using standard R_f/ϕ methods (Ramsay 1967, Dunnet 1969, Dunnet & Siddans 1971).

R_f/ϕ plots for marble breccias (Fig. 6) show the presence of a range of initial particle ratio (R_i) from 1:1 to 3:1. The ranges in R_i ratios are the same for all sections at each site suggesting the absence of a pre-deformational fabric. In order to evaluate the initial breccia fabric, the strained distributions of the breccias were undeformed using the procedure (program THETA) described by Peach & Lisle (1979). The method superimposes a coaxial strain having its long axis at right angles to the preferred orientation on the R_f/ϕ distribution. The magnitude of this superimposed strain is incremented and after each step the randomness of the resultant undeformed orientation of the markers is calculated. If no initial fabric is present, the reciprocal finite strain value can be determined from the strain necessary to bring about the most uniform particle distribution.

The chi-square test for randomness using this procedure and the initial distributions of the breccias (on a R_i/θ plot) are shown in Fig. 6. It is seen from the R_i/θ plots that the breccia long axes, as well as the range of R_i values, is randomly distributed in each section. The range in R_i values in the different sections also agrees with that determined from the R_f/ϕ plots. It is inferred that no predeformational fabric existed in these marble breccias (Fig. 5e), a conclusion in agreement with the geometries actually observed in the undeformed Apennine breccias.

Although the time-consuming R_f/ϕ method gives accurate results it was decided to try a more practical method of measurement in the field in order to obtain a wider distribution of sampling sites. Accordingly, the harmonic mean of 30–50 breccia axial ratios was determined (Lisle 1977) and the average angle that the long axes make with the reference direction (ϕ) was estimated for each section. Data collected using this method were found to give similar results to those collected using the above, more time consuming methods, even though a vector mean of long axes is not obtained as with the R_f/ϕ methods.

It is known that the harmonic mean gives a slight overestimate of the strain ratio (R_s) and that the initial particle shape can strongly affect the R_s value calculated using this method (Lisle 1979). For ranges in initial particle shape of $2.5 > R_i > 1.0$, significant overestimates of R_s only occur for R_s values less than 2.0 (Lisle 1979). The R_s values determined for each section using the harmonic mean method are almost always greater than 2.0 (Table 1). Therefore, for the range of initial breccia shapes observed (Fig. 6) the harmonic mean method provides a reasonable, rapid estimate of the tectonic strain ratio in these rocks. The R_s values for the remaining sites were then calculated using this method.

The results of all two-dimensional strain analyses, including the type of method used to determine the R_s values, are presented in Table 1. The R_s values for the reduction spots measured were calculated using the geometric mean of the R_f ratios of about 30 spots measured on principal planes of the strain ellipsoid.

Table 1. Two-dimensional strain data (marble breccias). Method used indicated by: (1) R_f/ϕ curves, (2) θ curve method of Peach & Lisle (1977), (3) harmonic mean of R_f values, (4) geometric mean of R_f values. Dip direction is 90° clockwise from strike; pitch of long axis taken clockwise from strike

Site	Section	N	Method used	R_s	Strike	Dip	Pitch
1 Tavolini	A	50	3	4.43	185	17	4
	B	50	3	6.25	10	90	0
	C	49	3	5.29	100	90	36
2 Bancaio Alto	A	50	3	2.23	184	89	143
	B	42	3	4.36	81	90	42
	C	40	3	2.39	0	0	149
3 Sotto Volegno I	A	50	3	2.07	136	20	44
	B	50	3	3.76	310	79	170
	C	50	3	6.06	37	90	177
4 Sotto Volegno II	A	50	3	2.87	152	90	25
	B	50	3	2.83	54	85	33
	C	35	3	2.12	8	27	172
5 Vagli Sopra	A	50	3	2.99	110	90	50
	B	50	3	3.02	290	2	47
	C	10	3	3.05	316	48	91
6 Colonnata	A	50	3	3.07	36	90	140
	B	50	3	3.17	120	90	131
	C	46	3	4.06	105	90	127
7 Ussaccio	A	51	3	4.22	106	90	43
	B	20	3	3.43	8	10	0
	C	44	3	3.17	10	90	10
9 Campocecina	A	53	1, 3, 4	6.32	335	75	173
	B	77	1, 3, 4	3.35	320	5	169
	C	20	1, 3, 4	6.58	70	90	161
8–11 Porcinacchia	A	52	1, 3, 4	4.08	140	14	10
	B	31	1, 3, 4	3.14	185	36	109
	D	52	1, 3, 4	5.04	65	90	123
13 S. Giuliano	A	31	3	3.01	66	90	3
	B	30	3	2.32	135	35	120
	C	30	3	2.31	168	50	155
	D	30	3	2.05	95	41	165
	E	30	3	2.37	207	68	142
14 Piastraccia	A	56	3, 2, 1	7.63	57	90	96
	B	84	3, 2, 1	3.61	358	16	124
	C	59	3, 2, 1	2.56	304	90	95
15 Punta Bianca	A	40	3	2.26	34	16	155
	B	40	3	4.97	5	88	170
	C	31	3	3.41	246	70	0
	D	41	3	4.10	227	90	8
	E	34	3	2.27	122	15	65
16 Faniello Est	A	140	3	4.15	180	88	178
	B	115	3	5.47	198	85	190
	C	86	3	3.60	130	43	2
17 Cava al Corchia	A	50	3	4.13	323	67	169
	B	24	3	1.85	106	22	40
	C	50	3	6.25	63	90	3
18 Faniello Nord	A	85	3, 4	4.62	100	13	30
	B	70	3, 4	8.52	86	89	30
	C	72	3, 4	5.11	343	90	14
19 Endorie	A	50	3	2.72	340	85	147
	B	50	3	3.45	67	90	137
	C	46	3	2.92	15	90	136
20 Cava la Terza	A	50	3	4.47	47	90	48
	B	46	3	2.78	167	87	5
	C	50	3	3.59	292	85	125
	D	70	3, 2, 4	2.98	344	90	176
	E	50	3, 2, 4	6.33	83	90	49
	F	200	3, 2, 4	3.99	40	90	42
22 Sopra Arni	A	50	3	2.67	80	24	130
	B	43	3	4.75	88	90	142
	C	6	3	6.81	162	90	153
24 Piscinicchi	A	38	3	3.61	336	90	7
	B	49	3	6.52	68	90	140
	C	26	3	7.06	36	90	145
25 Cervaiole	A	93	3, 2, 1	5.01	151	90	49
	B	63	3, 2, 1	2.35	60	90	85
	C	114	3, 2, 1	2.14	60	1	95

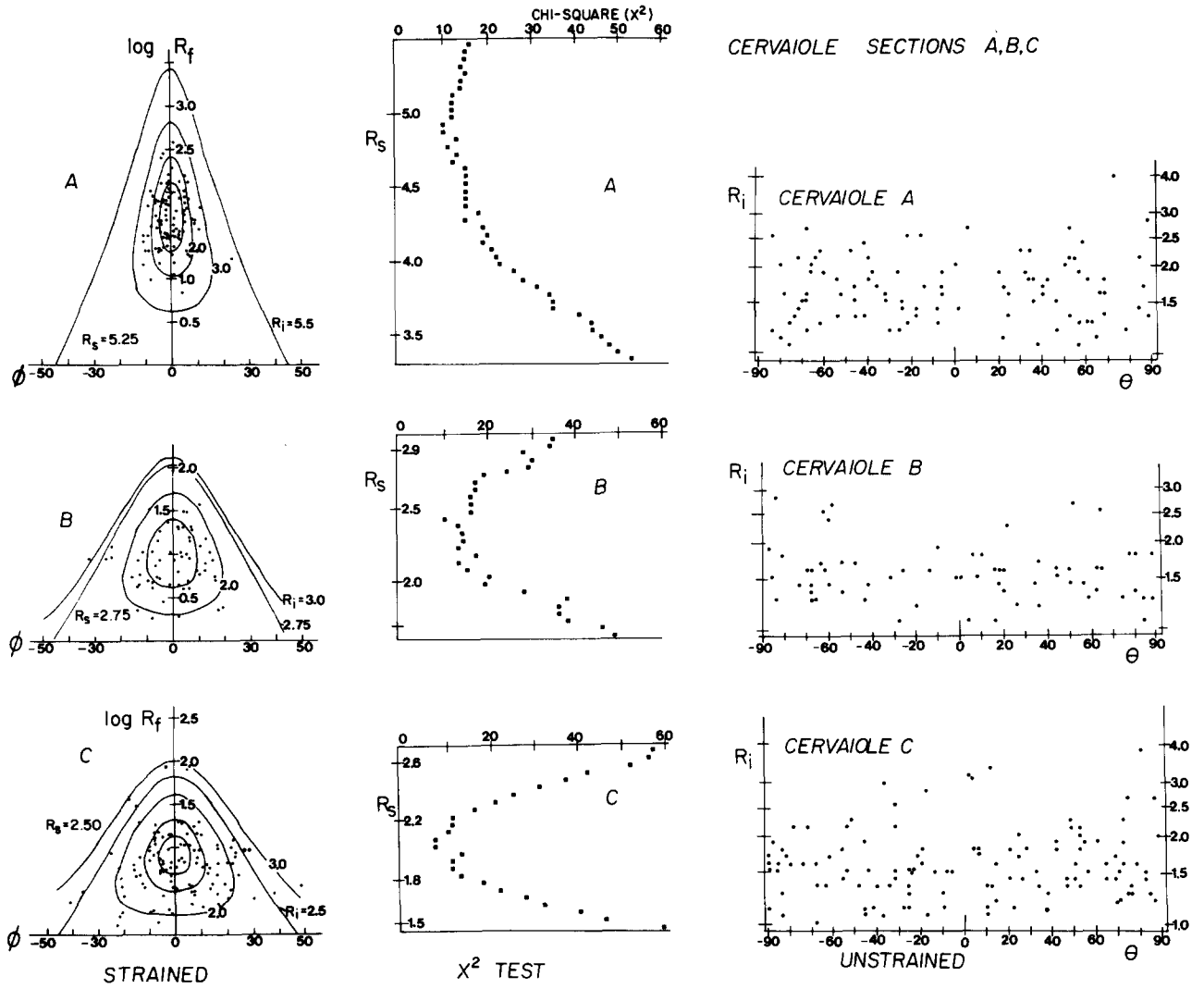

Fig. 6. Two-dimensional strain analyses of three different planar sections from locality 25. The R_f/ϕ method of Dunnet (1969) has been used to fit curves of equal initial particle ratio (R_i) to the strained distributions (left side). These strained distributions have been unstrained using the method of Peach & Lisle (1979). The resultant chi-square tests (centre) and unstrained R_i/θ distributions (right) are indicated.

Three-dimensional strain analyses

The strain data from the planar sections have been combined to obtain the values and directions of the finite strain in three dimensions. In general, we have combined data from three or more, non-principal, non-perpendicular planar sections. It has been previously demonstrated that analysis of three-dimensional, homogeneous, finite strain using ellipsoidal objects can be made on any section planes, including those that are not principal planes of the finite strain ellipsoid (Ramsay 1967, p. 147, Milton 1980, Siddans 1980).

The strain ellipsoid was calculated using a program written by Owens. The program scales ellipse data from the different sections so that all data sets refer to a common ellipsoid. The ellipsoid is calculated from the scaled ellipses by solving a set of simultaneous, linear equations, which have as unknowns, the 6 independent coefficients of the ellipse tensor specified with respect to the reference axes. Three sections give 7 equations for 6 unknowns. The solution of the linear equations is done using a routine for the accurate least squares solution for an overdetermined set of linear equations. The resultant matrix is then diagonalized to find the principal values and directions of the strain ellipsoid. The measured ellipse on each section is compared with that derived from the calculated ellipsoid. The calculated ellipsoid is used to unstrain the measured ellipsoid, and the log mean of the unstrained ellipses (r) is calculated and provides a measure of the reliability of the strain solution (a log mean of r = 1.00 is expected for a perfect solution).

The principal directions and values of the strain ellipsoid for selected sites are plotted on stereograms together with the sectional input data, the S_1 schistosity trace and the L_1 lineation (Fig. 7). Wherever a range of solutions was possible (due to the overdetermined nature of the data) the ellipsoid values and directions were chosen in order to minimize the value of r and so that the

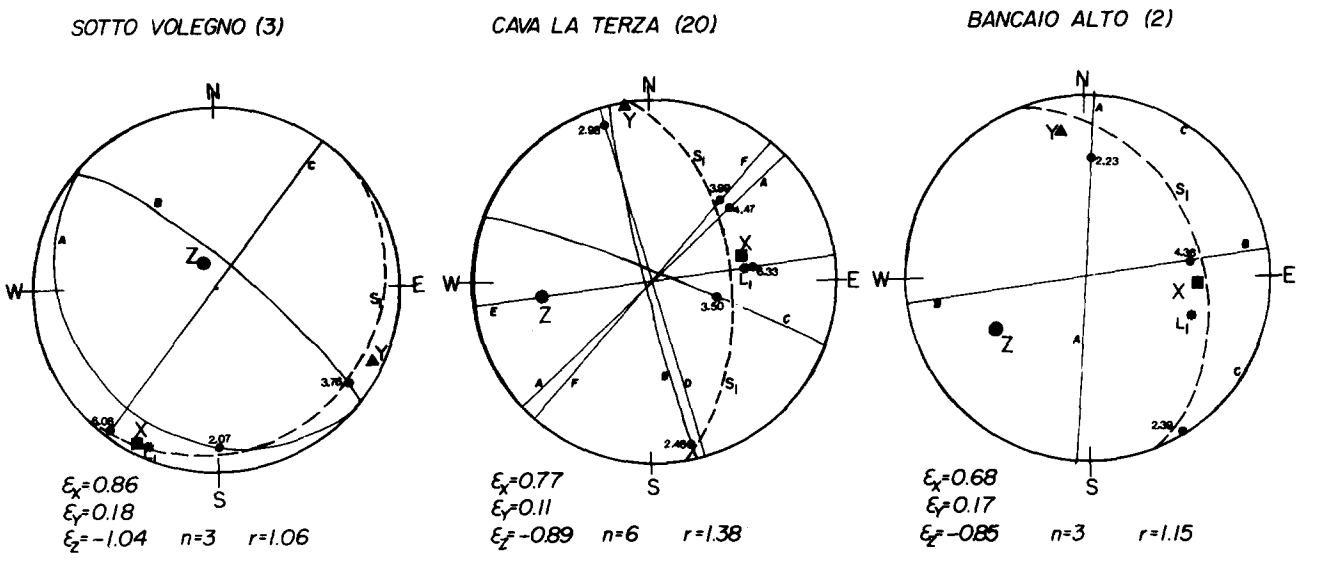

Fig. 7. Three-dimensional strains determined from two-dimensional data. For each site the tectonic strain ratios (R_s) and its orientation for three or more planar sections have been used to determine the three-dimensional finite strain. The traces in lower hemisphere, equal-area projection of the planar sections (A, B, C, etc.) and their respective R_s values are indicated. $\varepsilon_x > \varepsilon_y > \varepsilon_z$ = principal finite logarithmic strains. r = log mean of the undeformed ellipse ratios on two-dimensional sections. n = number of planar sections. The trace of S_1 schistosity and L_1 lineation are shown.

X strain directions were as close to L_1 as possible. The principal values and directions of the strain ellipsoid together with r values for all sites are listed in Table 2.

Effect of refolding on finite strains

The large-scale geometry of the Alpi Apuane region is seen in the cross sections of Fig. 8. The S_1 schistosity and D_1 phase folds have been refolded during the D_3 deformation and the entire region now resembles a large scale antiform (Carmignani & Giglia 1979b). The X:Z ratios derived from the finite strain data of Table 2, assuming equal-volume ellipsoids, are shown in the profiles of the S_1 schistosity. In order to interpret these data, the geometric effects of this late-stage deformation must now be investigated.

Any finite strain must be the product of the incremental strains due to each deformation phase. For analytical purposes it is convenient to decompose the strain into symmetric and skew-symmetric parts relating to the irrotational (distortion and volume change) and rotational strains, respectively (Ramsay 1967, p. 282). The nature of the finite strain caused by the superposition of the D_3 phase strain on that of the D_1 phase depends on the

Table 2. Three-dimensional strain data (marble breccias). $\varepsilon_x > \varepsilon_y > \varepsilon_z$ are principal logarithmic strains where $\varepsilon_i = \ln(1 + e_i)$. r = log mean of undeformed ellipses (see text). $K = (\varepsilon_1 - \varepsilon_2)/(\varepsilon_2 - \varepsilon_3)$.

Site	ε_x	Az	Dip	ε_y	Az	Dip	ε_z	Az	Dip	r	K
1	0.701	031	14	0.464	130	32	−1.166	280	54	1.12	0.15
2	0.680	238	44	0.167	349	21	−0.846	096	39	1.15	0.51
3	0.856	207	5	0.184	117	10	−1.036	324	79	1.06	0.67
4	0.698	180	5	0.164	086	41	−0.862	276	49	1.09	0.52
5	1.135	059	55	−0.102	153	3	−1.033	245	35	1.27	1.33
6	0.519	239	50	0.351	347	15	−0.870	088	36	1.06	0.14
7	1.010	044	32	0.104	152	26	−1.113	273	46	1.12	0.74
8	0.641	261	63	0.502	158	7	−1.142	065	26	1.20	0.08
9	1.136	105	10	0.179	192	18	−1.315	043	69	1.10	0.64
11	0.858	179	39	0.354	300	33	−1.212	056	39	1.14	0.32
12	0.378	–	–	0.148	–	–	−0.545	–	–	–	0.33
13	0.404	276	47	0.050	041	27	−0.453	148	30	2.18	0.70
14	1.108	189	84	0.007	302	3	−1.115	032	6	1.12	0.98
15	0.875	196	10	0.030	105	6	−0.906	347	79	1.10	0.90
16	1.172	071	3	0.148	161	1	−1.320	266	87	1.11	0.70
17	1.189	202	4	0.152	112	10	−1.341	315	79	1.06	0.69
18	0.889	082	31	0.427	343	15	−1.316	231	55	1.06	0.27
19	0.479	230	46	0.283	132	8	−0.763	034	43	1.11	0.19
20	0.774	079	50	0.112	349	1	−0.887	258	40	1.38	0.66
22	1.013	261	41	−0.147	353	3	−0.866	087	49	2.05	1.61
24	0.836	222	36	0.342	324	16	−1.178	074	49	1.07	0.33
25	1.230	149	49	−0.375	342	41	−0.855	247	6	1.00	3.34

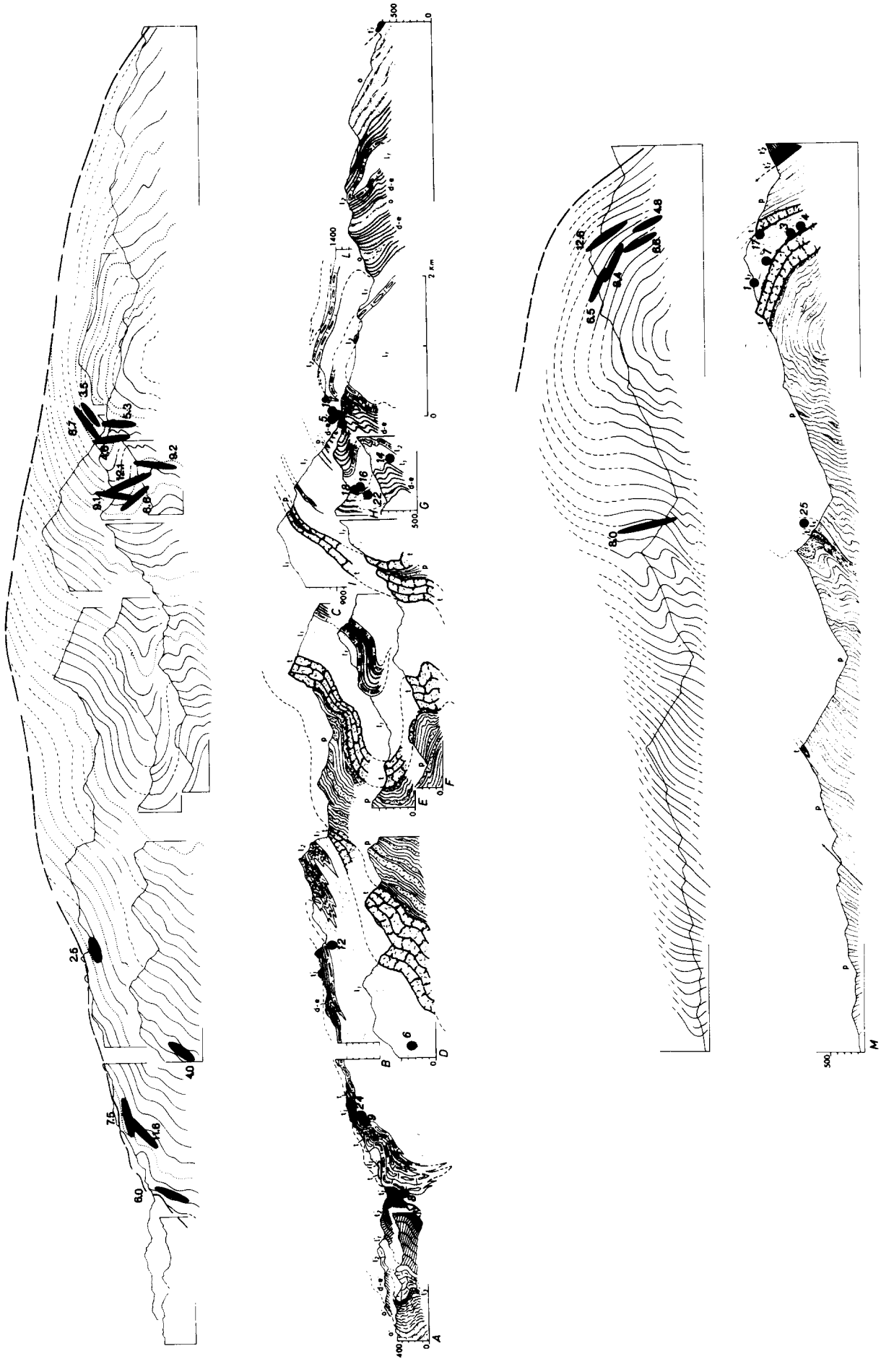

Fig. 8. Cross sections across the Alpi Apuane region showing locations of sites where strain determinations were obtained. Key to symbols: *P*, Palaeozoic strata; other symbols as in Fig. 2. Upper sections show trace of S_1 schistosity in an WSW–ENE, *XZ* section. The *X*/*Z* ratios of the strain ellipsoids are indicated. Localities 8, 9, 24, 12 and 6 comprise Group W from the non-rotated region while sites 1, 7, 3, 4, 17 comprise group E from the rotated region (discussed in text).

mechanism of folding during D_3. We envisage two end-member situations.

(1) The D_3 deformation is accommodated by flexural–slip folding with little irrotational strain occurring within the centres of the layers. In such a case the finite strain values record mostly the D_1 phase strains.

(2) During D_3, buckling developed with internal deformation accommodated by tangential longitudinal strain (or by flexural–flow folding). The finite strain ratio is then the product of the strains from both phases.

The geometric effects of these models are illustrated in Fig. 10 where strain ellipses have been constructed to reflect a D_1 phase simple shear geometry whose schistosity makes an initial angle of 45° to the layering (Fig. 9a). Deformation of this geometry by flexural–slip folding (Fig. 9b) produces ellipses whose final ratios reflect mostly the strain of the D_1 phase. Deformation by buckling with tangential longitudinal strain (Fig. 10c) produces finite strain ellipses whose ratios and orientations must vary according to position within the late-stage fold. Comparison of the observed geometry (Fig. 8) with these elementary models suggests that on a large scale only the D_1 phase strain ratios at sites 2, 5, 14, 16, 18, 22 and 25 would be seriously modified by the D_3 deformation. The remaining sites could be expected to reflect the finite strain of the D_1 phase, as do the majority of marble breccia shapes previously discussed. We therefore maintain that the measured strains at the majority of sites largely reflect the geometry of the D_1 deformation phase. It is therefore appropriate to investigate the relationships between the finite strain values and orientations and the geometry of the D_1 deformation phase.

FINITE STRAIN RESULTS

All finite strain data have been plotted on a logarithmic deformation plot (Fig. 10). The values of the parameters $K = (\varepsilon_1-\varepsilon_2)/(\varepsilon_2-\varepsilon_3)$ are in Table 2.

The reduction spots were measured from the vicinity of marble breccia localities 2, 5, 19 and 20 (Fig. 8). We note that the finite strains determined from the reduction spots (slates) are similar in their order of magnitude and style (K-values) to those determined from nearby marble breccias. The oncalites of site 12 (dolomitic marble) however, record a lower strain magnitude than nearby breccias but are of similar shape (K-value).

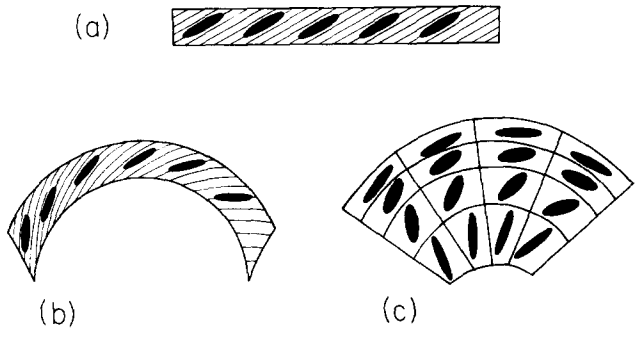

Fig. 9. Effects of late-stage refolding on D_1 phase strains. (a) Strain ellipses and orientations produced during D_1 phase, largely by simple shear. (b) Passive rotation of D_1 phase strain ellipses due to late-stage flexural slip folding. The finite strain values reflect the D_1 deformation; only their orientations are changed during refolding. (c) Buckling of D_1 phase geometry with internal distortion accommodated by tangential longitudinal strain. The finite strains shown are the product of D_1 phase strains and late-stage strains. Compare with profiles of Fig. 8.

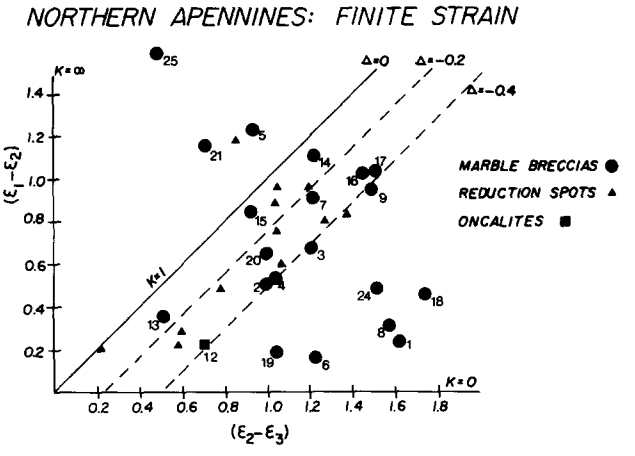

Fig. 10. Logarithmic deformation plot of Northern Apennine finite strain values. $\varepsilon_1 > \varepsilon_2 > \varepsilon_3$ are principal logarithmic strains: $\varepsilon_i = \ln(1+e_i)$. Localities of numbered sites shown in Figs. 4 and 8. Sites 13 and 15 are at Mt. Pisano and Punta Bianca, respectively (see Fig. 1). All other sites are in Alpi Apuane. Straight lines of volume loss (Δ) during pure shear deformation are indicated and separate the deformation field of true flattening ($0 < K < 1$) from that of true constriction ($1 < k < \infty$) where $K = (\varepsilon_1 - \varepsilon_2)/(\varepsilon_2 - \varepsilon_3)$.

In Fig. 10, ellipsoids of true flattening type (ε_2 positive) and true constriction type (ε_2 negative) are separated by those of plane strain ($\varepsilon_2 = 0$) by the line having unit slope given by:

$$\varepsilon_1-\varepsilon_2=\varepsilon_2-\varepsilon_3+\ln(1+\Delta)$$

where Δ is the finite volume change (Ramsay & Wood 1973). The data show large departures from the plane strain condition which can be ascribed to two different processes: (1) a true departure from plane strain accommodated by physical elongation in the Y direction; or (2) the superposition of volume loss and/or a homogeneous strain on a plane strain.

If departure from the $K = 1$ (and $\Delta = 0$) line is due entirely to extension along the Y direction then very large changes in Y from +50% to +250% are required. There is no evidence of such elongations parallel to Y from field studies. Folds are not extended parallel to Y, fibres around pyrites as well as vein systems show extension along X but not parallel to Y. In the absence of any convincing field evidence for physical elongations of this order of magnitude parallel to Y, we conclude that it is more useful to examine other models. In particular there is ample evidence to regard the region as an overthrust zone (Carmignani *et al.* 1978). Simple shear associated with overthrust zones results in plane strain ellipsoids. Deviations from plane strain can be ascribed to the effects of combinations of simple shear with accompanying volume loss and/or superposed longitudinal strain (Ramsay 1980). It is therefore appropriate to see if the observed strains can be accounted for by the combined effects of these processes.

Much of the data in Fig. 10 lie in the field of apparent flattening ($1>K>0$) between lines representing 0 and 40% volume loss. These lines apply to the finite strain state regardless of how this volume loss occurred (i.e. from simple shear, pure shear or any other process). It is therefore not possible to use this plot to consider separately the relative contributions of simple shear, pure shear and volume loss during the build-up of the finite strains. In the next section alternative methods are presented which enable a comparison to be made of the observed strains with those expected from various combinations of simple shear, pure shear, and volume loss.

Heterogeneous simple shear

The progressive rotation of fold axes into the extension direction during D_1 deformation led Carmignani *et al.* (1978) to propose that a component of simple shear strain was responsible for the observed geometries. In simple shear, the orientations of the principal axes of the finite strain ellipse and the strain ratio (R) depend on the amount of shear (γ) (Ramsay 1967, p. 88).

The strain data from the Alpi Apuane region can be divided into a western zone of non-rotated folds (sites 6, 8, 9, 12 and 24 of Figs. 4 and 8) and an eastern zone of rotated or sheath folds (the remaining sites). The K values from the western non-rotated zone range from 0.14 to 0.64 whereas those from the rotated regions range from 0.15 to 3.34. Thus although there is a tendency for the K value to be low in the non-rotated region, K values of all types are found in the rotated region. At 12 sites from two different areas (localities 6, 8, 9, 12, 24 in the west and localities 5, 19, 1, 7, 3, 4, 17 in the east) we have measured θ', the angle the major axis of the strain ellipse makes with the nappe boundary; we estimate that the values are reliable to $\pm 15°$ accuracy. At all other localities, the uncertainties due to the D_3 refolding make any meaningful measurements impossible.

For simple shear alone, the relationship between strain ratio (R) and (θ') the angle the long axis makes with the shear zone boundary is shown by the curve of Fig. 11. The Alpi Apuane data plotted on this graph do not lie on the curve and we can conclude that simple shear alone cannot account for the observed strains.

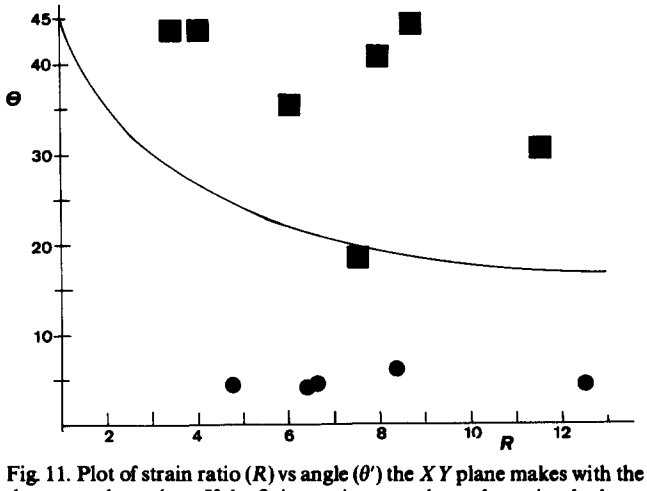

Fig. 11. Plot of strain ratio (R) vs angle (θ') the XY plane makes with the shear zone boundary. If the finite strains were due only to simple shear, the plotted points would lie on the curve. Data from the eastern and western groups of sites are shown as circles and squares respectively.

Simple shear and volume change

We now describe the displacement fields of simple shear (γ) followed by a volume change (Δ) acting normal to the shear zone walls. The deformation gradient matrix in the shear zone is (Ramsay 1980):

$$\begin{vmatrix} 1 & 0 & \gamma \\ 0 & 1 & 0 \\ 0 & 0 & 1+\Delta \end{vmatrix} \tag{1}$$

From this, the strain ratio (R) and the angle (θ') which the strain long axis makes with the shear zone boundary can be expressed as functions of γ and Δ. The equations (derived from equations 17, 19 and 20 in Ramsay (1980)) are:

$$R = \frac{\gamma^2+1+(1+\Delta)^2+(1+\gamma^2+(1+\Delta)^2-4(1+\Delta)^2)^{1/2}}{\gamma^2+1+(1+\Delta)^2-(1+\gamma^2+(1+\Delta)^2-4(1+\Delta)^2)^{1/2}}, \tag{2}$$

$$\tan 2\theta' = \frac{2\gamma(1+\Delta)}{1+\gamma^2-(1+\Delta)^2}. \tag{3}$$

From (2) and (3) it is also possible to express γ and Δ in terms of R and θ'. This is presented graphically on the strain chart of Fig. 12, from which values of simple shear (dashed lines) and volume change can be determined directly.

Strain data from the western (non-rotated) zone are shown as squares and those from the rotated zone as circles. It is seen that volume changes of ± 70–80% are required to account for these strains if only simple shear and volume change are involved. It is also expected that the value of γ would increase as folds become rotated into the extension direction during a simple shear process. However the values of γ from the rotated area are less than those from the non-rotated area.

It is concluded that simple shear with volume change alone cannot account for the observed strains. We note that reversing the order of the matrix multiplication (to volume change followed by simple shear) changes the shapes of the curves slightly, but not their overall pattern.

Combined simple shear and pure shear

The finite strains can be factorized into a shear strain (γ) in the direction of shear and an additional longitudinal strain (λ) in this direction (Matthews *et al.* 1971). This can be expressed by the deformation gradient matrix

$$\begin{vmatrix} \sqrt{\lambda} & 0 & \gamma/\sqrt{\lambda} \\ 0 & 1 & 0 \\ 0 & 0 & 1/\sqrt{\lambda} \end{vmatrix} \tag{4}$$

(Coward 1976, p. 184). From this the orientations (θ) and ratios (R) of the strain ellipse can be expressed in terms of γ

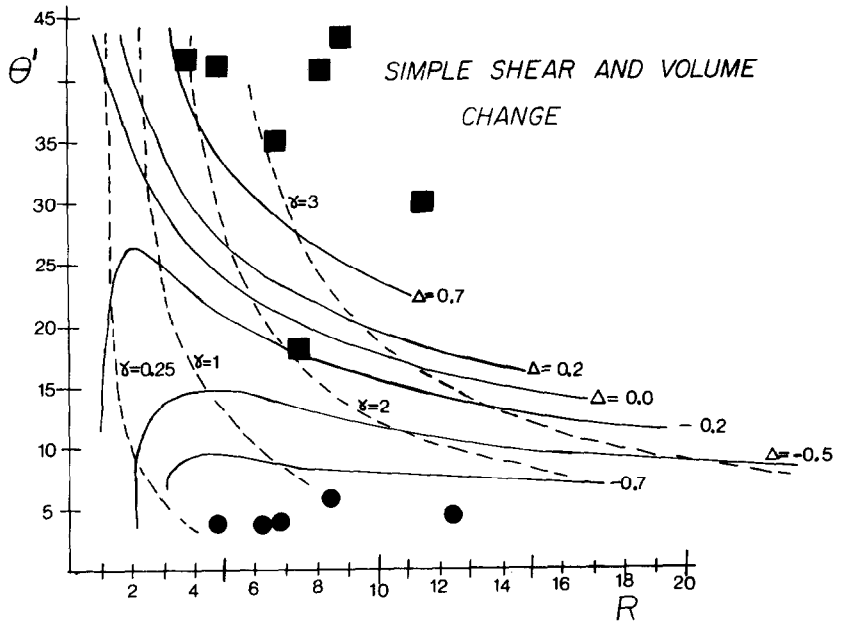

Fig. 12. Values of simple shear (dashed lines) and volume change (solid lines) plotted on the strain chart for varying finite strain ratios and orientations of the principal extension direction with respect to the shear zone boundary. Site symbols as in Fig. 11.

and λ. Using this method the Alpi Apuane data have been plotted on the strain chart of Fig. 13.

Values of λ in the shear direction from the western, non-rotated zone range from $0.6 > \lambda > 0.3$ while those from the rotated zone vary from $8.0 > \lambda > 2.0$. An increase in shear strain is evident from the non-rotated region ($0.8 > \gamma > 1.8$) towards the rotated region ($1.5 > \gamma > 8.5$). The analysis does not take into account volume change. The effect of changing the order of matrix multiplication (to simple shear followed by layer-parallel shortening) shifts the position of the γ curves somewhat, but not the λ curves (Coward & Kim 1981). The implications of these results are discussed below.

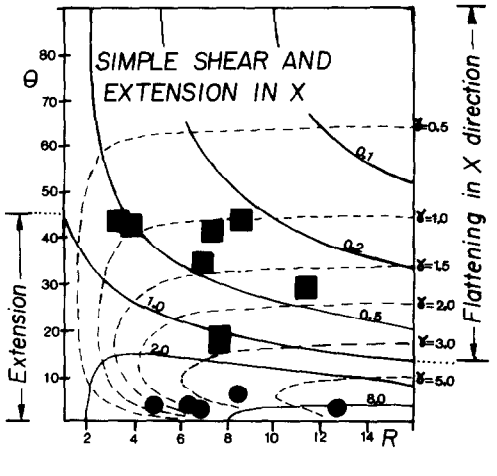

Fig. 13. Values of simple shear (dashed lines) and pure shear (solid lines) plotted on a strain chart for varying finite ratios (R) and orientations of the principal extensions (θ). Site symbols as in Fig. 11.

SUMMARY

The finite strains plotted in Fig. 10 have been considered in terms of simple shear alone (Fig. 11), simple shear with volume loss (Fig. 12), and simple shear with longitudinal strain (Fig. 13). The comparisons of the strain data with the models reveal that none of these models can completely explain the observed strains and their orientations. It appears that a combination of simple shear with additional longitudinal strain is best able to account for the data generated by the models considered.

Clearly it is necessary to consider the simultaneous operation of simple shear, pure shear, and volume change. The two-dimensional geometry on a shear zone profile for the deformation gradient matrix representing homogeneous strain, followed by simple shear and then volume change is

$$\begin{vmatrix} a+b\gamma & b+d\gamma \\ b(1+\Delta) & d(1+\Delta) \end{vmatrix} \quad (5)$$

where a, b and d represent the terms of the homogeneous deformation gradient matrix in the shear zone walls (Ramsay 1980). For the case of plane strain $b=0$ and $d = 1/a$ and the matrix further simplifies to:

$$\begin{vmatrix} a & \frac{\gamma}{a} \\ 0 & \frac{1+\Delta}{a} \end{vmatrix} \quad (6)$$

which can be expanded and solved in terms of the principal strains $(1+e_1)$ and $(1+e_2)$ and the angle θ' which the strain axes make inside the shear zone. Unfortunately we only have two independent variables,

the strain ratio $R = (1+e_1)/(1+e_2)$ and the angle θ' but three dependent variables to solve for (a, γ, Δ). We have therefore been unable to solve for the general case of γ, λ and Δ together using the Alpi Apuane data.

DISCUSSION

If the Alpi Apuane region is considered as a shear zone then we can use the above methods to describe the strain variation inside the zone. A general increase in γ from southwest to northeast is observed across the zone. At the same time a change is observed in the value of λ from $\lambda < 1.0$ in the southwest to $\lambda > 1.0$ in the northeast. This pattern is remarkably similar to that observed by Coward (1976) in the Botswana shear zone. Thus in both cases, there must have been deviation from simple shear: values of $\lambda < 1.0$ in the southwest would lead to a broadening of the shear zone and values of $\lambda > 1.0$ in the northeast would lead to a thinning of the shear zone. Perhaps inhomogeneous strains acting across the shear zone walls accompanied shear zone deformation. Unfortunately we do not have enough data to investigate the serious compatability problems that must arise from such a situation where the shear zone walls are curved.

Interestingly, when the plane strain condition is relaxed at shear zone terminations, it is possible to produce zones of flattening and constriction (Ramsay & Allison 1979) which somewhat resemble the Alpi Apuane strain pattern. In this scenario, the flattened western region might represent the southwest end of the shear zone where it ramps into the basement, while the constricted eastern region might represent the end of the shear zone where it ramps into overlying strata (Fig. 15, discussed below).

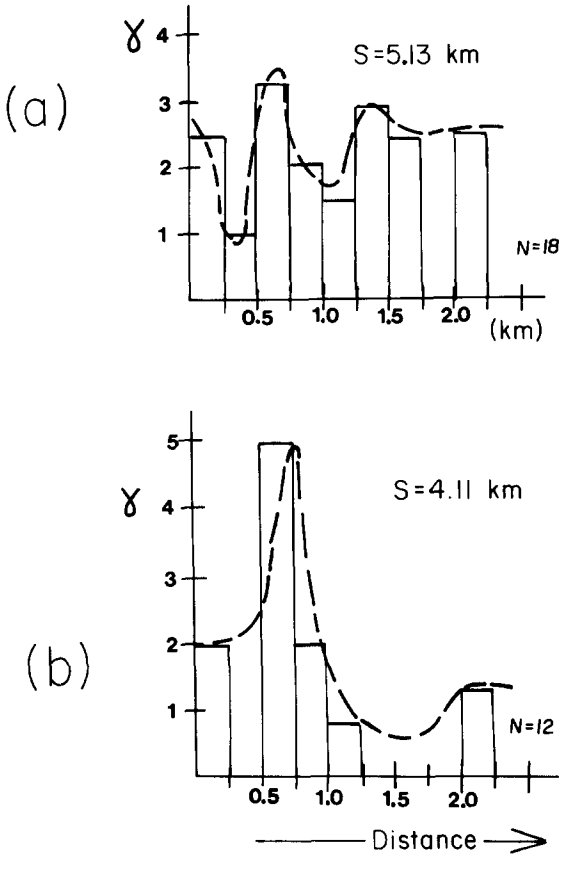

Fig. 14. Shear strain (γ)-distance plots derived from analysis of S_1 schistosity profiles (Fig. 8) and finite strain ratios (Table 2). The total shear stress (s) across the zone has been estimated by integrating variations in γ. (a) Calculated assuming only simple shear. (b) Calculated assuming simple shear and extension in the shear direction. See text for discussion. N, number of sites used in calculations.

Displacement during shear

Assuming the above analyses provide a rough guide to the natural situation, the displacement across the shear zone can be calculated by integrating values of γ as a function of distance(s) from the shear zone boundary (Ramsay & Graham 1970). Shear strain-distance plots have been drawn for the model of simple shear alone (Fig. 14a) and for a model of simple shear with longitudinal strain (Fig. 14b). In the latter case the values of γ used are those derived from the strain plot of Fig. 13. The total displacement calculated from the latter model is 4.11 km and must be regarded as a minimum displacement because no strain readings were included from deeper levels in the shear zone due to the effects of D_3 refolding.

Length of deformation and strain rates

The total time (t) available for the sequence of deformation phases (D_1 to D_3) in the Alpi Apuane region is 15 Ma. This figure is derived from the difference between the K/Ar and Ar^{40}/Ar^{39} ages associated with the D_1 phase (26 Ma) and the dates associated with the youngest events (11 Ma) (Kligfield *et al.* 1977, 1980).

An order of magnitude estimate of the average strain rate can be made by combining the finite strain data of Table 2 with the total time of 15 Ma available for the progressive deformation.

Extensional strains ranging from $2.42 > e_1 > 0.46$ and shortening strains of from $|-0.74| > e_3 > |-0.36$ result in strain rates of $5.11 > \dot{e} > 0.96 \times 10^{-15}$ sec^{-1} for extension and $1.56 > \dot{e} > 0.76 \times 10^{-15}$ sec^{-1} for shortening. If most of this strain was accumulated during the D_1 phase, then even less time was available. Assuming a figure of 8 Ma (1/2 the total available time) for the duration of the D_1 phase, strain rates of $9.58 > \dot{e} > 1.82 \times 10^{-15}$ sec^{-1} and $2.93 > \dot{e} > 1.42 \times 10^{-15}$ sec^{-1} for extension and shortening, respectively, are obtained.

In a summary compilation of all available finite strain data, Ramsay & Pfiffner (1981) report variations in strain rate from 3×10^{-14} to 10^{-5} sec^{-1}. They note that strains do not accumulate linearly with time, but that strain rate depends also on the type of incremental strain (i.e. simple vs pure shear). They present a family of theoretically derived strain rate curves (R) vs time (Ramsay & Pfiffner in press). The Alpi Apuane data lie between the strain rate curves of 10^{-14} sec^{-1} and 10^{-15} sec^{-1}, in agreement with the theoretical considerations of Ramsay & Pfiffner.

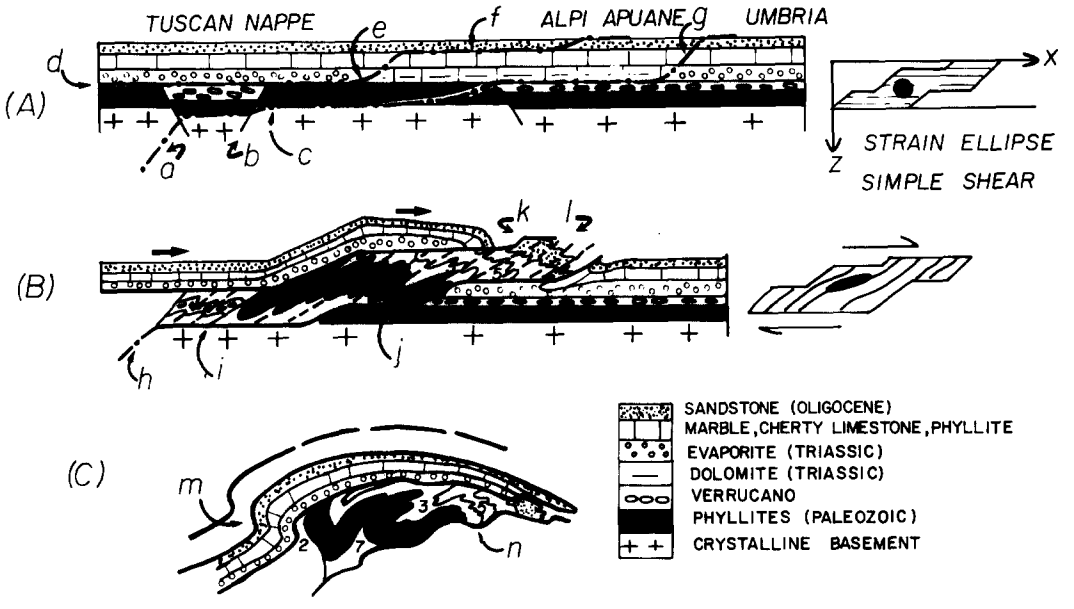

Fig. 15. Simple shear geometry and tectonic evolution of the Alpi Apuane region during the Oligocene–Miocene. (A) Initiation of shear zone by development of flat–ramp–flat geometry: a, possible ductile shear zone passing into crystalline basement; b, initial orientation of normal faults, grabens in Massa region; c, possible décollement of Palaeozoic phyllites above crystalline basement; d, décollement beneath evaporite layer creates Tuscan nappe; e, ramp at Triassic facies change from evaporite to dolomite; f, flat under Oligocene sandstones; g, frontal ramp of shear zone lower boundary. (B) Initial overthrusting of Tuscan nappe and ductile deformation in shear zone: h, postulated shortening of crystalline basement by heterogeneous, ductile shear; i, deformed orientation of graben showing resultant position of Massa unit on top of Alpi Apuane sequences; j, modification of early-formed ramp folds and buckles of competent horizons by simple shear; k, asymmetric distribution of lithologies within shear zone results from shear folding of initial ramp–flat geometry; l, schistosity within shear zone develops at 45° angle to shear zone boundary and is progressively shallowed as shear continues. (C) Refolding of Alpi Apuane region during Oligocene–Miocene. m, refolding of nappe contacts; n, ductile refolding and smoothing of initial ramp–flat geometry.

Tectonic implications

A series of cartoons depicting the evolution of the Alpi Apuane region is presented in Fig. 15. The models account for many of the geometric features observed. Palaeozoic basement consists largely of phyllites, quartzites and schists previously involved in the Hercynian orogeny. These rocks presumably overlie a pre-Hercynian crystalline basement, although no outcrops are presently known. We suggest that at deeper levels, shortening of this presumed crystalline basement may have been accomplished by ductile shear (Fig. 15a). At higher levels the shortening was accommodated by the formation of thrust sheets whose boundaries were defined by the typical ramp–flat geometries shown (Figs. 15c–g). During continued shortening, the thrust sheet was affected by simple shear along its boundaries and developed into a shear zone. The asymmetric distribution of lithologies (*k*) within the zone is a direct consequence of the initial ramp–flat geometry of the boundaries. The structures that developed inside the shear zone include low angle schistosities making initial 45° angles to the shear zone boundaries (*l*) and mineral extension lineations in the direction of the finite strain ellipse. Buckle folds developed due to the compressive stresses that acted along the lithological layering in the shear regime. These buckle folds, along with folds formed by the ramping of competent layers (Fig. 15j) were then modified by progressive simple shear and extended parallel to the *X* strain direction, often forming sheath folds.

A preliminary idea of the crustal shortening can be calculated by balancing the cross section of Fig. 15 along the level of the Triassic evaporite and dolomite. The distance between the northeasternmost piece of Triassic of the Tuscan nappe (which was originally to the southwest of the Alpi Apuane region) and the southwesternmost Triassic of the metamorphic sequences is 28 km, giving a minimum displacement for the overlying Tuscan nappe of 28 km. When combined with the measured displacement in the shear zone of 4 km, a total displacement of 32 km is involved. If the crystalline basement took part in this deformation, a minimum basement shortening strain of 21% in this part of the Apennines is expected.

Rifting and extension during the Mesozoic caused widespread crustal thinning of the Apennine continental margin (D'Argenio & Alvarez 1980). During the collisional deformation described in this paper, rethickening of this strongly thinned, heterogeneous continental crust (D'Argenio & Kligfield 1980) resulted in a Northern Apennine crust of normal thickness of only 30–35 km (Giese & Morelli 1975).

This predeformation crustal thickness can be estimated from the strain results using the relationship:

$$t_0 = (1+e_1)t$$

where t_0 is the original thickness, e_1 the shortening strain across the continental margin, and t the present observed thickness. The results indicate that the predeformation North Apennine thicknesses ranged from 19 to 23 km,

that is in good agreement with the models of Helwig (1976), Giess *et al.* (1970), and D'Argenio & Alvarez (1980).

Acknowledgements—We thank Drs. S. Schmid, M. Casey and J. G. Ramsay for reviews of the manuscript, and the undergraduates following the course of structural geology at Pisa for assistance with fieldwork. This work was partially supported by Swiss National Science Foundation grant 5.521.330.622/8 and by the Centro di Geologia Strutturale e Dinamica dell Appennino Settentrionale, (CNR Pisa) (L.C.).

REFERENCES

Bernoulli, D., Kälin, O. & Patacca, E. 1979. A sunken margin of the Mesozoic Tethys: the Northern and Central Apennines. Symposium "Sédimentation jurassique W. européen" *A.S.F. Publication spéciale No.* 1, *March* 1979. 197–210.

Carmignani, L. & Giglia, G. 1977. Le fasi tettoniche terziare dell' Autoctono delle Alpi Apuane: studio delle strutture minori della zona centro-meridionale. *Boll. Soc. geol. Ital.* **94**, 1957–1981.

Carmignani, L. & Giglia, G. 1979a. Analasi mesostrutturale della zona occidentale delle Apuane Metamorfiche. *Boll. Soc. geol. Ital.* **96**, 429–450.

Carmignani, L. & Giglia, G. 1979b. Large-scale reverse "drag folds" in the late Alpine building of the Apuane alps (N. Apennines). *Atti Soc. tosc. sci. nat. Mem. Ser. A* **86**, 109–125.

Carmignani, L., Giglia, G. & Kligfield, R. 1978. Structural evolution of the Apuane Alps: an example of continental margin deformation in the Northern Apennines, Italy. *J. Geol.* **86**, 487–504.

Cobbold, P. R. & Quinquis, H. 1980. Development of sheath folds in shear regimes. *J. Struct. Geol.* **2**, 119–126.

Colacicchi, R., Pialli, G. & Praturlon, A. 1975. Megabreccias as a product of tectonic activity along a carbonate platform margin. Extraits des Publications du Congrès Ixème Congrès International de Sédimentologie. Nice, 1975, 61–68.

Coward, M. P. 1976. Strain within ductile shear zones. *Tectonophysics* **34**, 184–197.

Coward, M. P. & Kim, J. H. 1981. Strain within thrust sheets. In: *Thrust and Nappe Tectonics* (edited by McClay, K. R. & Price, N. J.) *Spec. Publ. geol. Soc. Lond.* **9**, 275–292.

D'Argenio, B. & Alvarez, W. 1980. Stratigraphic evidence for crustal thickness changes on the southern Tethyan margin during the Alpine Cycle. *Bull. geol. Soc. Am.* **91**, 681–689.

D'Argenio, B. & Kligfield, R. 1980. Crustal thinning and its effect on the collisional deformation of continental margins: the Apennine example. *26th Int. geol. Congr. Paris Abstr.* **1**, 326.

Dunnet, D. 1969. A technique of finite-strain analysis using elliptical particles. *Tectonophysics* **7**, 117–136.

Dunnet, D. & Siddans, A. W. B. 1971. Non-random sedimentary fabrics and their modification by strain. *Tectonophysics* **12**, 307–325.

Escher, A. & Watterson, J. 1974. Stretching fabrics, folds and crustal shortening. *Tectonophysics* **22**, 223–231.

Giese, P. & Morelli, C. 1975. Crustal Structure of Italy. Quaderni de "La ricerca Scientifica" **90**, 453–489, C.N.R., Rome.

Giese, P., Günther, K. & Reutter, K. J. 1970. Vergleichende geologische und geophysikalische Betrachtungen der Westalpen und des Nordapennins. *Z. dt. geol. Ges.* **120**, 151–195.

Giglia, G. & Trevisan, L. 1966. Genesi e significato paleogeografico delle brecce tra Grezzoni e marmi delle Alpi Apuane. *Atti Soc. tusc. sci. nat., Mem. Ser. A.* **73**, 503–517.

Giannini, E. & Lazzarotto, A. 1975. Tectonic evolution of the Northern Apennines. In: *Geology of Italy.* (edited by Squyres, C.) Earth Sci. Soc. of Libyan Arab Republic, Tripoli **1**, 237–287.

Helwig, J. 1976. Shortening of continental crust in orogenic belts and plate tectonics. *Nature, Lond.* **260**, 768–770.

Kligfield, R. 1979. The Northern Apennines as a collisional orogen. *Am. J. Sci.* **279**, 676–691.

Kligfield, R., Hunziker, J. & Schamel, S. 1977. K/Ar ages of multiply deformed metasedimentary rocks from the Alpi Apuane, Northern Apennines and their tectonic significance (Abs.) In: *Proc. 5th Eur. Congr. Geochron. Cosmochron. Isotope Geol.* Pisa, 5–9 September, 1977.

Kligfield, R., Hunziker, J. Dallmeyer, R. D. & Schamel, S. 1980. Implicazioni tettoniche dell' éta assolut a (K/Ar e $^{40}Ar/^{39}Ar$) di metasedimenti a deformazione multiplà delle Alpi Apuane. (Abs.) In: Riassunti, Societa Geologica Italiana, 70° Congresso, Siena 6–11 Oct. 1980: L'evoluzione tettonico-sedimentario dell'appennino settentrionale, 4–5.

Lisle, R. 1977. Estimation of the tectonic strain ratio from the mean shape of deformed elliptical markers. *Geologie Mijnb.* **56**, 140–144.

Lisle, R. 1979. Strain analysis using deformed pebbles: the influence of initial pebble shape. *Tectonophysics* **60**, 263–277.

Logan, B. W., Rezak, R. & Ginzburg, R. N. 1964. Classification of algal stromatolites. *J. Geol.* **72**, 68–63.

Matthews, P. E., Bond, R. & Van den Berg, J. 1971. Analysis and structural implications of a kinematic model of similar folding. *Tectonophysics* **12**, 129–154.

Milton, N. J. 1980. Determination of the strain ellipsoid from measurements on any three sections. *Tectonophysics* **64**, T19–T27.

Peach, C. J. & Lisle, R. J. 1979. A Fortran IV program for the analysis of tectonic strain using deformed elliptical markers. *Comput. Geo-Sci.* **5**, 325–334.

Ramsay, J. G. 1967. *Folding and Fracturing of Rocks.* McGraw-Hill, New York.

Ramsay, J. G. 1980. Shear zone geometry: a review. *J. Struct. Geol.* **2**, 83–99.

Ramsay, J. G. & Allison, I. 1979. Structural analysis of shear zones in an alpinised Hercynian granite (Maggia Lappen, Pennine Zone, Central Alps). *Schweiz. Miner. petrogr. Mitt.* **59**, 251–279.

Ramsay, J. G. & Graham, R. H. 1970. Strain variation in shear belts. *Can. J. Earth Sci.* **7**, 786–813.

Ramsay, J. G. & Pfiffner, O. A. in press. Constraints on geological strain rates: arguments from finite strain states of naturally deformed rocks. *J. geophys. Res.*

Ramsay, J. G. & Wood, D. S. 1973. The geometric effects of volume change during deformation processes. *Tectonophysics* **16**, 263–277.

Rau, A. & Tongiorgi, M. 1974. Geologia dei Monti Pisani a sud-est della Valle del Guappero. *Mem. Soc. geol. Ital.* **13**, 227–408.

Rhodes, S. & Gayer, R. A. 1977. Non-cylindrical folds, linear structures in the *X* direction and mylonite developed during translation of the Caledonian Kalak Nappe Complex of Finnmark. *Geol. Mag.* **114**, 329–408.

Sanderson, D. J. 1973. The development of fold axes oblique to the regional trend. *Tectonophysics* **16**, 55–70.

Siddans, A. W. B. 1980. Analysis of three-dimensional, homogeneous, finite strain using ellipsoidal objects. *Tectonophysics* **64**, 1–16.

Williams, G. D. 1978. Rotation of contemporary folds into the *X* direction during overthrust processes in Laksefjord, Finnmark. *Tectonophysics* **48**, 29–40.